J. Chem. Sci. Vol. 123, No. 4, July 2011, pp. 509–516.

CO adsorption on ionic Pt, Pd and Cu sites in $Ce_{1-x}M_xO_{2-\delta}$ ($M = Pt^{2+}, Pd^{2+}, Cu^{2+}$)

GARGI DUTTA[a], ASHA GUPTA[b], UMESH V WAGHMARE[a] and M S HEGDE[c,*]

[a]Theoretical Sciences Unit, Jawaharlal Nehru Centre for Advanced Scientific Research, Jakkur Campus, Bangalore 560 064, India

[b]Materials Research Centre, Indian Institute of Science, Bangalore 560 012, India

[c]Solid State and Structural Chemistry Unit, Indian Institute of Science, Bangalore 560 012, India

e-mail: mshegde@sscu.iisc.ernet.in

MS received 7 November 2010; revised 30 March 2011; accepted 5 April 2011

Abstract. Noble metal ion substituted CeO_2 in the form of $Ce_{0.98}M_{0.02}O_{2-\delta}$ solid solution (where M = Pt, Pd, Cu) are the new generation catalysts with applications in three-way exhaust catalysis. While adsorption of CO on noble metals ions is well-known, adsorption of CO on noble metal ions has not been studied because creating exclusive ionic sites has been difficult. Using first-principles density functional theory (DFT) we have shown that CO gets adsorbed on the noble metal Pt^{2+}, Pd^{2+}, Cu^{2+} ionic sites in the respective compounds, and the net energy of the overall system decreases. Adsorption of CO on metal ions is also confirmed by Fourier transform infrared spectroscopy (FTIR).

Keywords. Noble metal ion; density functional theory; FTIR; ceria.

1. Introduction

Abatement of CO emission is a growing concern because it is one of the main components of auto exhaust gases. Noble metals like Pd, Pt, Rh, Ru, Cu, dispersed on various oxide supports, are known to adsorb and help in oxidation of CO in presence of oxygen. Exhaust catalysis and CO oxidation was largely restricted to noble metals dispersed on oxide supports like Al_2O_3.[1–11] Hegde *et al.* in their account 'Noble metal ionic catalyst' have shown the effect of substituting noble metal ions in CeO_2 and TiO_2 supports on exhaust catalysis.[12] When oxide supports are doped with lower valent noble metal ions, it creates oxygen vacancies in the support oxide to balance the overall charge. The study on CO oxidation by $Au_xCe_{1-x}O_2$ catalyst (using standard DFT and DFT+U methods), shows the weakening of the oxide by the presence of dopant. The Au dopant weakens the bonds of the surrounding oxygens making the catalyst a better oxidant, hence facilitating CO oxidation.[13,14] In principle, electron deficient substituted metal ions provide active sites for CO adsorption, whereas the molecular O_2 gets adsorbed on the neighbouring oxide ion vacancy. In our work, noble metal ion substituted catalysts such as $Ce_{1-x}M_xO_{2-\delta}$ ($M = Pt^{2+}$, Pd^{2+}, Cu^{2+}) provide pathway for electron transfer from CO to O_2 via Ce–O bond in the dual site catalyst and such structures are stable. Oxidation of CO in these catalysts, $Ce_{1-x}M_xO_{2-\delta}$, occurs by taking O from dissociated O_2 formed at the surface oxide ion vacancy. While adsorption of CO on Pt^0, Pd^0 atoms dispersed in oxide support is well-known and well-studied, CO adsorption on noble metal ions in a reducible oxide needs to be studied. Bera *et al.* have studied primary CO adsorption on Pt^{2+} ion in CeO_2 and showed that the sticking probability of CO on Pt ion is about the same as that on Pt^0 in Pt metal.[15] Since rates of CO oxidation over noble metal ions substituted CeO_2, TiO_2 are orders of magnitude higher than the corresponding noble metal nanoparticles dispersed on Al_2O_3, an understanding of CO adsorption on noble metal ions is essential.

Here we report first-principles Density Functional Theory (DFT) calculations for stabilization of Pt^{2+}, Pd^{2+} and Cu^{2+} ions in $Ce_{1-x}M_xO_{2-\delta}$ (M = Pt, Pd and Cu respectively). We have investigated adsorption of CO on metal ion sites substituted in CeO_2 by DFT calculations and confirmed this by FTIR studies.

*For correspondence

2. Methods

2.1 *Experimental*

2% M^{2+} Substituted CeO_2 (where $M = Pt^{2+}$, Pd^{2+}, Cu^{2+}) have been synthesized by solution combustion method. The combustion mixture for the preparation of 2% Pt/CeO_2 contained $(NH_4)_2Ce(NO_3)_6$, H_2PtCl_6 and $C_2H_5NO_2$ (glycine) in the molar ratio 1:0.02:2.67. In a typical preparation, 5.4823 g (0.01 moles) of $(NH_4)_2Ce(NO_3)_6$ (E. Merck India Ltd., 99.9%), 0.105 g (2.03×10^{-4} moles) of $H_2PtCl_6.6H_2O$ (Sigma Aldrich) and 2.002 g (0.0267 moles) of glycine (Merck, 99%) were dissolved in 30 ml volume of water in a 300 ml crystallizing dish. The dish with mixture was then introduced into a preheated furnace maintained at 350°C. The combustion started after dehydration and the product was obtained in 60 seconds. Similarly, 2% Pd/CeO_2 and 2% Cu/CeO_2 were synthesized by combustion method and precursors used were $PdCl_2$ and $Cu(NO_3)_2$ respectively. All the samples were characterized by powder X-ray diffractometer (XRD) (Philips X'Pert Diffractometer fitted with graphite crystal monochromator, Cu Kα radiation). In our earlier studies, we have carried out extensive structural studies of these compounds with XRD, XPS, TEM and EXAFS and showed that these noble metal ions are substituted for Ce^{4+} ions in CeO_2 and forms a solid solution. Pt is mainly present as Pt^{2+} ion in 2%Pt/CeO_2, Pd as Pd^{2+} ion in 2%Pd/CeO_2 and Cu as Cu^{2+} ion in 2% Cu/CeO_2 and compounds are represented by the formula $Ce_{0.98}Pt_{0.02}O_{2-\delta}$, $Ce_{0.98}Pd_{0.02}O_{2-\delta}$ and $Ce_{0.98}Cu_{0.02}O_{2-\delta}$ respectively.[16–18]

FTIR spectra of CO over $Ce_{0.98}Pt_{0.02}O_{2-\delta}$, $Ce_{0.98}Pd_{0.02}O_{2-\delta}$ and $Ce_{0.98}Cu_{0.02}O_{2-\delta}$ were recorded on a Thermo Fisher Scientific Nicolet 380 FTIR equipped with an *in situ Diffuse Reflectance Infra-red Fourier Transform* (DRIFT) chamber and a high sensitivity MCT detector. The spectra were recorded in the 650–4000 cm^{-1} wave number region at a resolution of 4 cm^{-1} with an accumulation of 100 scans. 30 mgs of the samples were made into a pellet of 2 mm diameter which was heated in air for 2 h at 150°C prior to recording DRIFT spectrum. The cell is connected to a conventional gas handling system. *In situ* heating of the samples at 120°C was carried out under N_2 flow for 30 minutes, and then after cooling down to room temperature reference spectrum was recorded under same N_2 flow. At room temperature 5% CO balanced in Nitrogen was passed over the sample at a flow rate of 30 cc/min.

2.2 *Theory*

We performed total energy calculations using the ABINIT[19,20] implementation of DFT.[21] While the LDA+U type of corrections are known to be important in reduced form of ceria[22] and also use of hybrid functionals, we are mainly interested in the atomic structure which is expected to be less sensitive to these corrections. The use of LDA+U makes the calculations more costly, especially when using large number of atoms for slab calculations. In this work, we are not interested in the electronic structure, hence we use standard DFT–LDA approach. Compounds based on ceria, which involve mixed valence of cerium, exhibit large number of competing local minima of electronic total energy. As the energy differences between the states are small, the ground state can be difficult to access.[22] The addition of U-term to the LDA functional facilitates access to the physical ground state by enhancing its stability. Physical results, however, were found to be insensitive to the value of U-parameter.[22] In fact, LDA results have been found to be better than GGA results by Fabris *et al.*[22] We have studied both bulk and surface using the standard LDA–DFT approach for substituted and reduced ceria.[23–25] It solves the Kohn–Sham equations[26] by a fixed potential-based conjugate-gradient minimization[27] of one-electron energies in the ground-state and iteratively determines the self consistent potential.[28] The potential of the nucleus and the core electrons was approximated with pseudopotentials–optimized pseudopotentials were used for Ce, O, Pt, Pd,[29] Trouiller–Martins pseudopotential for Cu and Goedecker–Teter–Hutter pseudopotential for C. Plane wave basis with energy cut-off of 25 Ha to represent Kohn–Sham wavefunction, a $2 \times 2 \times 2$ Monkhorst–Pack grid for sampling Brillouin Zone integration[30] and exchange-correlation energy within a local density approximation (LDA[31]) were used. Ionic relaxations were performed using a Broyden, Fletcher, Goldfarb, Shanno (BFGS)-based minimization[32] and also using molecular dynamics with viscous damping. Hirshfeld atomic charge analysis was performed to understand the net charge on atoms and charge transfers between atoms.[25,33]

Simulations of CeO_2 (100) surfaces were done with supercells of 16 formula units, $Ce_{16}O_{32}$, (figure 1) containing a symmetrical slab of CeO_2 and both surfaces of the slab are oxygen terminated (in order to cancel the intrinsic dipole moment which would have arose due to different terminations, O on one surface and Ce on the other). In order to maintain the correct formula units, we have created 50% O-vacancy on

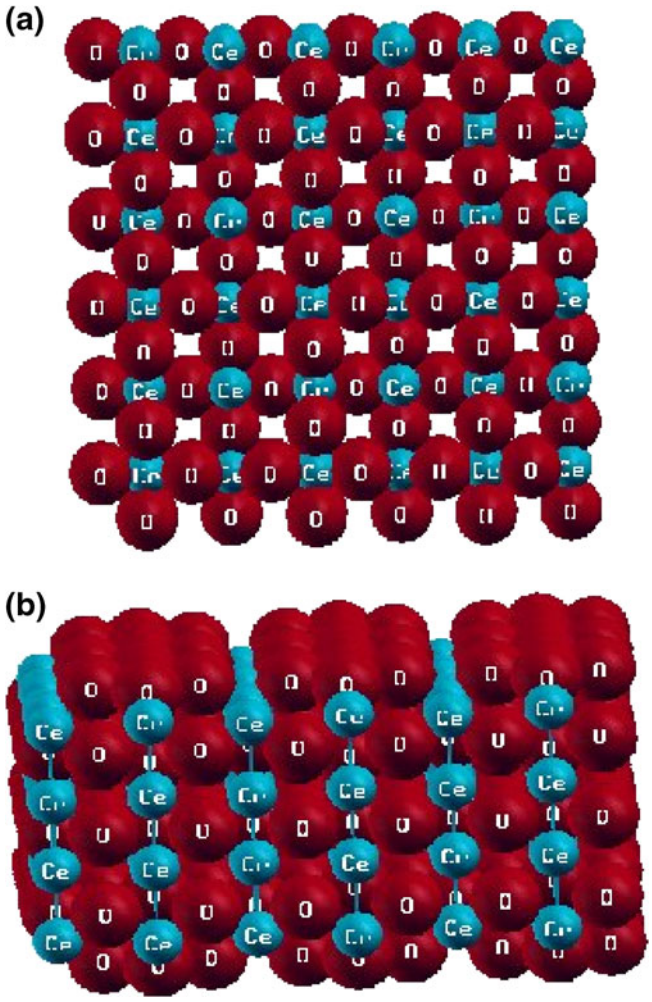

Figure 1. Structures of pure CeO_2: (**a**) top view of slab, (**b**) side view of slab.

one surface and removed the oxygens to the other surface. So both the surfaces have 50% O-vacancy and the occupied oxygen sites are same on both surfaces. Skorodumova *et al.*[34] discussed various models of oxygen termination for the CeO_2 (100) surface. The model for the slab (100 surface) of substituted ceria has been earlier used by us to study hydrogen spillover on $Ce_{1-x}Pt_xO_{2-x}$ 25 Since the solid solutions form cubic nano-crystallites, in which the (100) surface is mostly exposed, we chose to study reactions over the (100) surface in our theoretical investigations. The details of the slab model have been discussed earlier by us.[25]

We have taken $Ce_{15}PtO_{31}$ supercell where one Ce has been substituted for Pt and an oxygen vacancy has been created in the layer below that of Pt to maintain the charge balance in the supercell. Similar models of $Ce_{15}PdO_{31}$ and $Ce_{15}CuO_{31}$ were used for simulating Pd and Cu doped surfaces. Due to the partial O-vacancy on the surfaces, Pt/Pd/Cu ions are exposed to the surface even though it is in the second layer of atoms in the slab. Cerium and oxygen layers are stacked in the z-direction and we have used sufficient vacuum thickness of about 15–17 Å in our calculations to keep the slab–slab interaction negligible. CO molecule is adsorbed on the surface of doped ceria to study the stability and adsorption sites of CO.

3. Results and discussion

All freshly prepared noble metal ion doped CeO_2 were characterized by powder XRD and XPS and matched with our earlier reports.[17,18] The Pt, Pd and Cu ions substituted CeO_2 are represented by the solid solutions $Ce_{0.98}Pt_{0.02}O_{2-\delta}$, $Ce_{0.98}Pd_{0.02}O_{2-\delta}$ and $Ce_{0.98}Cu_{0.02}O_{2-\delta}$. The DRIFT spectra of the $Ce_{0.98}Pt_{0.02}O_{2-\delta}$, $Ce_{0.98}Pd_{0.02}O_{2-\delta}$ and $Ce_{0.98}Cu_{0.02}O_{2-\delta}$ under 5% CO balanced in N_2 flow are shown in figure 2. $Ce_{0.98}Pd_{0.02}O_{2-\delta}$ shows two main bands at 2173 and 2087 cm^{-1}. $Ce_{0.98}Cu_{0.02}O_{2-\delta}$ shows two bands at 2174 and 2096 cm^{-1}. $Ce_{0.98}Pt_{0.02}O_{2-\delta}$ shows three main bands at 2173, 2099 and 2057 cm^{-1}. The bands at 2173 ± 1 cm^{-1} for $Ce_{0.98}Pd_{0.02}O_{2-\delta}$, $Ce_{0.98}Cu_{0.02}O_{2-\delta}$ and $Ce_{0.98}Pt_{0.02}O_{2-\delta}$ are due to physisorbed CO on the surface of the sample, which is close to ν(CO) at 2172 cm^{-1}. The band at 2087 cm^{-1} for $Ce_{0.98}Pd_{0.02}O_{2-\delta}$ is attributed to CO adsorbed on top of oxidized Pd^{2+} present on the surface. The band at 2096 cm^{-1} for

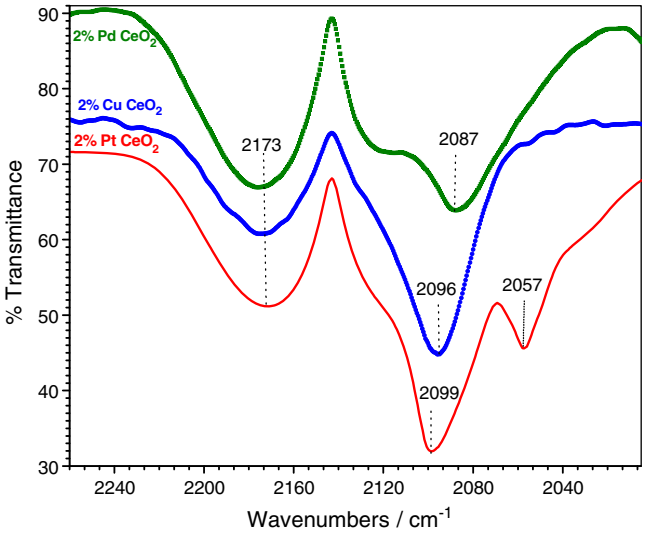

Figure 2. FTIR spectra of $Ce_{0.98}Pt_{0.02}O_{2-\delta}$, $Ce_{0.98}Pd_{0.02}O_{2-\delta}$ and $Ce_{0.98}Cu_{0.02}O_{2-\delta}$.

$Ce_{0.98}Cu_{0.02}O_{2-\delta}$ is attributed to CO absorbed on top of Cu^{2+}.[35,36] The band at 2099 cm^{-1} for $Ce_{0.98}Pt_{0.02}O_{2-\delta}$ is attributed to CO adsorbed on Pt^{2+} ion. Since Pt ion substituted CeO_2 has 15% Pt in +4 state, the band at 2057 cm^{-1} may be due to CO adsorbed on Pt^{4+} ion.[37] There is a gradual shift in stretching frequency of C–O bond (ν(CO)) towards higher wavenumber for CO adsorbed on the noble metal sites, namely, the bands at 2087, 2096 and 2099 cm^{-1} for $Ce_{0.98}Pd_{0.02}O_{2-\delta}$, $Ce_{0.98}Cu_{0.02}O_{2-\delta}$ and $Ce_{0.98}Pt_{0.02}O_{2-\delta}$ respectively.

In this work, we are interested only in the surface layer of atoms as they are more important for catalytic activity than the bulk layers. The simulated metal ion doped ceria slabs show changes in surface geometry, mainly in terms of displacement of doped ions from the site of substitution. In $Ce_{15}PtO_{31}$, the Pt ion moves towards the oxygen vacancy site (figure 3); similar are the cases for Pd and Cu doping, with maximum displacement for Cu ion.

The adsorption of CO on the sites of doped ions is tested by placing CO approximately at a distance of 1.86 Å on top of Pt/Pd/Cu ions in the initial configurations. CO adsorbed on Pt doped system, sits almost on top of Pt with the Pt–C–O moiety moved towards the oxygen vacancy site (figure 4a). The Pd–C–O complex in Pd doped system moves away from the oxygen vacancy and on the opposite side of the site of ion substitution, with the adsorbed C–O bent towards the oxygen vacancy site (figure 4b). Cu–C–O moiety in Cu doped system moves towards the oxygen vacancy and the C–O bends away from the oxygen vacancy site (not shown). We considered different adsorption sites of CO for the Pt/Pd doped cases: on top of O (figure 5a), on top of an O-vacancy site and on top of Ce (figure 5b) in the initial configurations, in order to find out the most stable position of CO on metal ion doped CeO_2 surface. The CO molecule initially placed on top of oxygen and oxygen vacancy site, does not form any bond with the surface and the net energy is positive, indicating the decrease in stability of these CO adsorbed systems. CO initially placed on Ce, moves far away from Ce in the final configuration without forming any bond with the surface. The net energy for different configurations with CO at various sites for the Pt doped case is given by:

$$E_{tot}\,(Ce_{15}PtO_{31} + CO) - E_{tot}\,(Ce_{15}PtO_{31}) - E_{tot}\,(CO)\,,$$

where E_{tot} (CO) is the total energy of an isolated CO molecule. The energies for CO absorbed on Pt ion, oxide ion and at the O-vacancy site are −1.39, 2.29 and 1.90 eV respectively. Chemisorption energy of CO on metal surfaces and metallic overlayer structures have been studied by *ab initio* calculations by Hammer *et al.* and their calculated chemisorptions energy on Pt (111) is −1.45 eV, which is close to our obtained value for Pt^{2+} ion in ceria.[38] The net energy for the system with CO initially placed on Pt, shows an increase in stability of the system with formation of a C–Pt bond. The energies for CO adsorbed on Pd and Cu ions substituted CeO_2 show similar behaviour as the Pt ion doped CeO_2.

The coordination of oxygens around Pt in CeO_2–Pt system is 2 and the Pt–O distances increase upon adsorption of CO on Pt. In CeO_2–Pd, the coordination

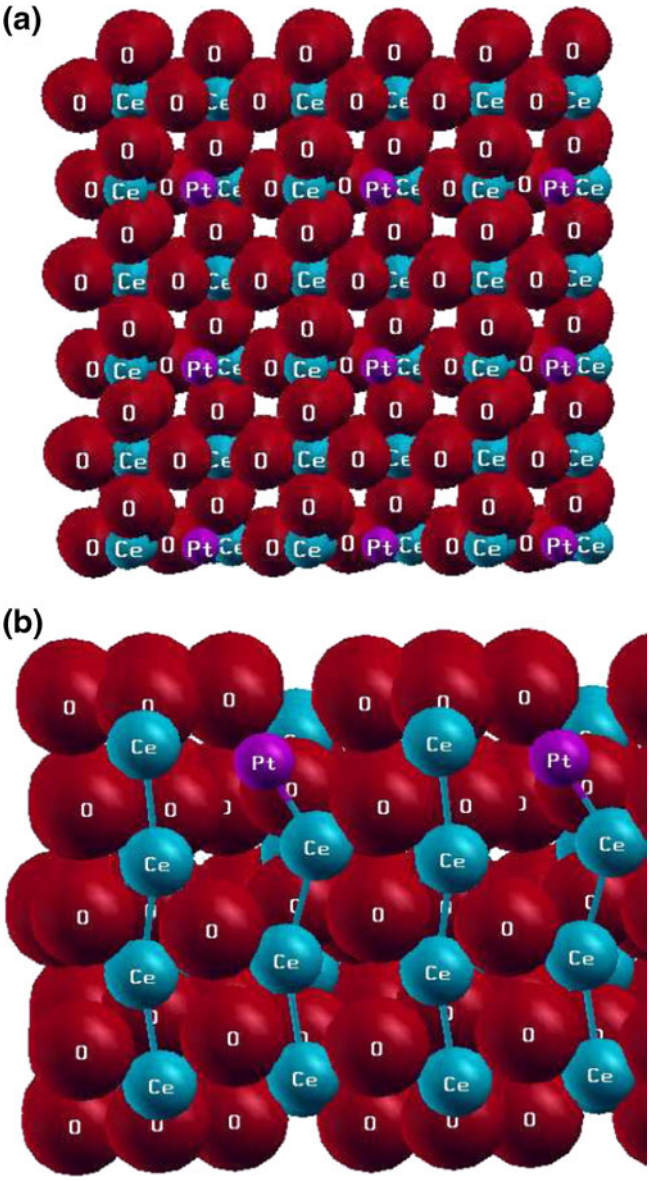

Figure 3. Structures of CeO_2/Pt: (**a**) top view of slab, (**b**) side view of slab (magnified).

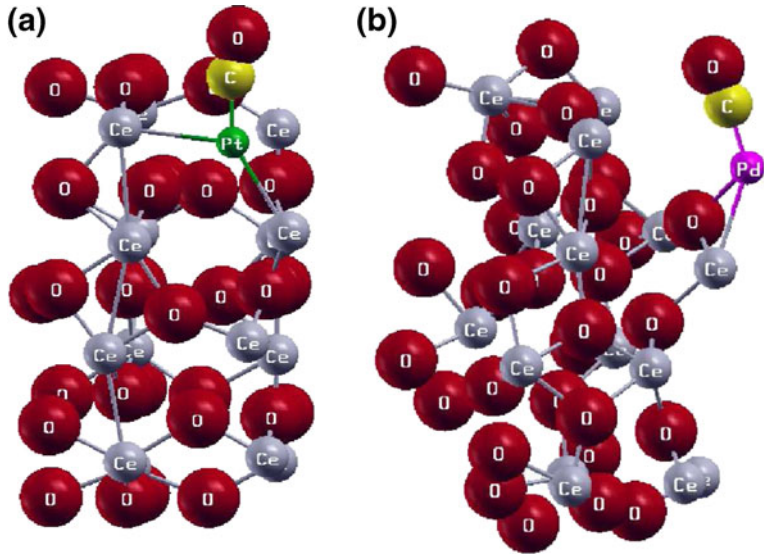

Figure 4. Structures of CO adsorbed on doped (**a**) Pt ion and, (**b**) Pd ion in CeO_2.

of oxygens around Pd is 3, and the Pd–O distances decrease upon CO adsorption. The coordination of oxygens around Cu in CeO_2–Cu is 4 of which 2 oxygens are weakly bonded and 2 oxygens are strongly bonded to Cu. On CO adsorption, the stronger Cu–O bonds become slightly weaker and the weaker Cu–O bonds become slightly stronger in Cu doped system. The Cu–O distances are least compared to Pt–O and Pd–O distances. We have specified all the nearby distances of Pt/Pd/Cu–O in CeO_2–Pt/Pd/Cu and CeO_2–Pt/Pd/Cu+CO systems to identify the coordination of the doped ions (see table 1). The net charge on Cu is maximum for the CeO_2–Cu case compared to the Pt/Pd doped cases. The charges on the surface ions change upon CO adsorption (see table 2). We discuss below the effect of CO adsorption for three different ions in detail.

3.1 *Case1: Pd–CeO_2*

The net positive charge is lowest on Pd (see table 2) which indicates that among the three metal ions Pd has more electron density. Upon CO adsorption the net positive charge on Pd slightly decreases but the net positive charge on Ce increases. This means Pd ion receives electron through Pd←C sigma bonding from CO and donates Pd→C back bonding. Since Pd has highest electron density among the three metal ions, this π-back bonding will be stronger and overall there will be net flow of electron towards CO. Also the net negative charge on O of CO is highest indicating flow of electron towards CO, as a result of which one should expect stronger Pd–C bond and weaker C–O bond.

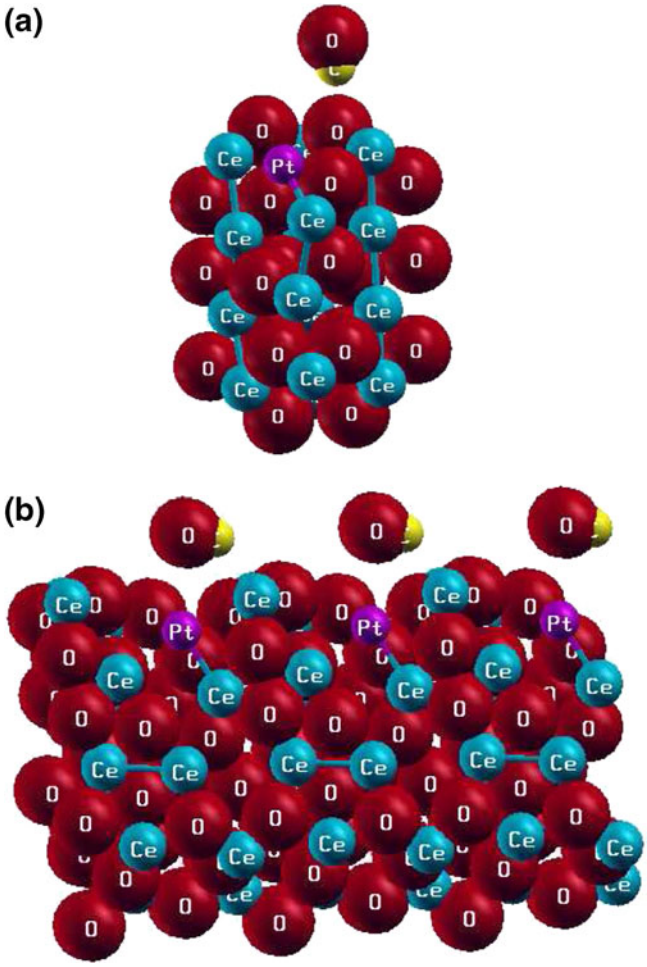

Figure 5. Relaxed configurations for CO initially placed at various sites of Pt doped CeO_2: (**a**) on oxygen (unit cell), (**b**) on Ce (extended structure).

Table 1. Shortest bond-length in CeO_2–Pt/Pd/Cu and CeO_2–Pt/Pd/Cu+CO (surface layer of atoms).

System	Type of bond	Shortest bond-length (Å)
CeO_2−Pt	Pt–O	(2.10, 2.10): coordination = 2
	Pt–Ce	2.66, 3.16
	Ce–Ce	3.21, 3.12, 3.34
CeO_2−Pd	Pd–O	(2.28, 2.28, 2.87): coordination = 3
	Pd–Ce	2.61, 3.77, 3.84
	Ce–Ce	3.21, 3.08, 3.36
CeO_2−Cu	Cu–O	(1.89, 1.89, 2.04, 2.04): coordination = 4
	Cu–Ce	2.72, 3.02, 3.03
	Ce–Ce	3.35, 3.43
CeO_2−Pt+CO	Pt–O	(2. 35, 2. 35): coordination = 2
	Pt–Ce	2.88, 3.00
	Ce–Ce	3.23, 3.07, 3.34
	C–O	1.14
	C–Pt	1.86
CeO_2−Pd+CO	Pd–O	(2.04, 2.23, 2.23): coordination = 3
	Pd–Ce	3.02, 3.03
	Ce–Ce	3.21, 3.19
	C–O	1.15
	C–Pd	1.82
CeO_2−Cu+CO	Cu–O	(1.90, 1.90, 1.92, 1.92): coordination = 4
	Cu–Ce	2.78, 2.92, 3.12
	Ce–Ce	3.33, 3.29
	C–O	1.17
	C–Cu	1.87
Pure CeO_2 (bulk)	Ce–O	2.36
Isolated CO	C–O	1.12

3.2 *Case2: Cu–CeO_2*

The case of Cu–CeO_2 is almost similar to that of Pd–CeO_2. There is an increase in net positive charge on Cu and decrease in net positive charge on Ce upon CO absorption. Due to π-back bonding there is a net flow of electrons towards CO. But the extent of this back bonding is lesser in this case compared to previous case. This is probably due to less electron density on Cu compared to Pd (see net charges on Pd and Cu before CO absorption). Net positive charge on C of Cu−CeO_2+CO system is higher compared to Pd−CeO_2+CO); O of CO has less negative charge due to very small flow of electrons towards CO. Therefore it is expected that Cu–C bonds will be less strong than Pd–C bond, and so in this case C–O bond is stronger compared to case above.

3.3 *Case3: Pt–CeO_2*

Upon CO adsorption, the net positive charge on both Pt and Ce decreases which implies that Pt is receiving electron through Pt←C bonding. There is drift of electron towards Pt–CeO_2 due to which C of CO becomes more positive and O of CO becomes less negative compared to previous two cases. Thus extent of back bonding is lesser compared to Pd and Cu substituted ions. Due to overall flow of electrons towards the oxide, Pt–C bond becomes weaker (less back bonding) and C–O bond becomes stronger and hence C–O stretching frequency should be stronger than Pd/Cu–CeO_2. Therefore, we expect the ν(CO) for CO adsorbed on these compound should increase in Pd<Cu<Pt order.

In FTIR spectra (figure 2) the band around $\sim$2090 cm^{-1} are attributed to ν(CO) for CO absorbed on top of $M^{\delta+}$ ion doped in ceria. The intensity of this band is strongest which indicates that CO is primarily adsorbed on metal ion sites. From DFT calculation we have seen that CO molecule adsorbed on metal ion doped in ceria is the stable structure, whereas CO molecule present at other sites like Ce^{4+} ion and oxide ion vacancy was not stable. The stretching frequency of C–O bond for CO adsorbed on top of Pd ion for Pd–CeO_2 sample is observed at 2087 cm^{-1}, for Cu−CeO_2 it appears at 2096 cm^{-1} and for Pt–CeO_2 it appears at 2099 cm^{-1}. So C–O stretching frequency is strongest for Pt–CeO_2 and weakest for Pd–CeO_2.

Table 2. Net charge on surface atoms (Pt/Pd/Cu doped side) in CeO_2−Pt/Pd/Cu and CeO_2−Pt/Pd/Cu+CO (average net charges on Ce, O).

System	Type of atom	Net charge
Pure CeO_2	Ce	0.7740
	O	−0.4309
CeO_2−Pt	Pt	0.3637
	Ce	0.7612
	O	−0.4195
CeO_2−Pd	Pd	0.3078
	Ce	0.7709
	O	−0.4196
CeO_2−Cu	Cu	0.3764
	Ce	0.8585
	O	−0.4525
CeO_2−Pt+CO	C	0.1235
	O (in CO)	−0.0405
	Pt	0.3163
	Ce	0.7492
	O	−0.4112
CeO_2−Pd+CO	C	0.0780
	O (in CO)	−0.0760
	Pd	0.2980
	Ce	0.7882
	O	−0.4248
CeO_2−Cu+CO	C	0.1039
	O (in CO)	−0.0412
	Cu	0.3814
	Ce	0.8186
	O	−0.4448

This stretching frequency of C–O thus follows the same trend as expected from DFT calculation.

This study clearly shows adsorption of CO on Pd^{2+}, Cu^{2+} and Pt^{2+} ions in CeO_2 matrix. Due to lower valent 2+ ion substitution for Ce^{4+} ion in ceria, an oxide ion vacancy is created. Among the three ions, ν_{CO} is lowest for Pd^{2+} ion. CO oxidation activity is highest for Pd^{2+} ion substituted CeO_2 compared to Cu^{2+} and Pt^{2+} ions substituted in CeO_2 (see table 8, ref.[39]). The difference in ν_{CO} is very small to claim that CO is strongly bonded to Pd^{2+} ion compared to Cu^{2+} and Pt^{2+} ions. However, higher adsorption propensity due to stronger adsorption over Pd^{2+} ion observed experimentally is indeed correlated with CO adsorption studies by DFT calculations.

4. Conclusions

Our first-principles calculations prove the stability of Pt/Pd/Cu ions in the ceria matrix. Indeed, Pt^{2+}, Pd^{2+} and Cu^{2+} ion substituted CeO_2 have been synthesized by the solution combustion method. DFT calculations show that CO binds only with Pt^{2+}, Pd^{2+} and Cu^{2+} ions present on the CeO_2 surface (see figures 4 and 5). CO binding on metal ions shown by DFT calculations is supported by experimental studies.

References

1. Bera P, Patil K C, Jayaram V, Hegde M S and Subbanna G N 1999 *J. Mater. Chem.* **9** 1801
2. Burch R and Watling T C 1997 *J. Catal.* **169** 45
3. Elmasides C, Kondarides D I, Grunert W and Verykios X E 1999 *J. Phys. Chem. B* **103** 5227
4. Galisteo F C, Mariscal R, Granados M L, Fierro J L G, Daley R A and Anderson J A 2005 *Appl. Catal. B* **59** 227
5. Gandhi H S, Graham G W and McCabe R W 2003 *J. Catal.* **216** 433
6. Harmsen J M A, Hoebink J H B J and Schouten J C 2001 *Chem. Eng. Sci.* **56** 2019
7. Kolli T, Rahkamaa-Tolonen K, Lassi U, Savimäki A and Keiski R L 2004 *Top. Catal.* **30–31** 341
8. Kosaki Y, Miyamoto A and Murakami Y 1982 *Bull. Chem. Soc. Jpn.* **55** 9
9. Macleod N, Isaac J and Lambert R M 2000 *J. Catal.* **193** 115
10. Rainer D R, Koranne M, Vesecky S M and Goodman D W 1997 *J. Phys. Chem. B* **101** 10769
11. Thomas J M 2008 *J. Chem. Phys.* **128** 182502
12. Hegde M S, Madras G and Patil K C 2009 *Acc. Chem. Res.* **42** 704
13. Nolan M, Verdugo V S and Metiu H 2008 *Surf. Sci.* **602** 2734
14. Shapovalov V and Metiu H 2007 *J. Catal.* **245** 205
15. Bera P, Patil K C, Jayaram V, Subbanna G N and Hegde M S 2000 *J. Catal.* **196** 293
16. Bera P, Gayen A, Hegde M S, Lalla N P, Spadaro L, Frusteri F and Arena F 2003 *J. Phys. Chem. B* **107** 6122
17. Bera P, Priolkar K R, Sarode P R, Hegde M S, Emura S, Kumashiro R and Lalla N P 2002 *Chem. Mater.* **14** 3591
18. Priolkar K R, Bera P, Sarode P R, Hegde M S, Emura S, Kumashiro R and Lalla N P 2002 *Chem. Mater.* **14** 2120
19. Goedecker S 1997 *SIAM J. Sci. Comp.* **18** 1605
20. Gonze X, Beuken J M, Caracas R, Detraux F, Fuchs M, Rignanese G M, Sindic L, Verstraete M, Zerah G, Jollet F, Torrent M, Roy A, Mikami M, Ghosez P, Raty J Y and Allan D C 2002 *Comp. Mater. Sci.* **25** 478
21. Hohenberg P and Kohn W 1964 *Phys. Rev.* **136** B864
22. Fabris S, de Gironcoli S, Baroni S, Vicario G and Balducci G 2005 *Phys. Rev. B* **71** 041102 (R)
23. Dutta G, Waghmare U V, Baidya T, Hegde M S, Priolkar K R and Sarode P R 2006 *Catal. Lett.* **108** 165
24. Dutta G, Waghmare U V, Baidya T, Hegde M S, Priolkar K R and Sarode P R 2006 *Chem. Mater.* **18** 3249

25. Dutta G, Waghmare U V, Baidya T and Hegde M S 2007 *Chem. Mater.* **19** 6430
26. Kohn W and Sham L J 1965 *Phys. Rev.* **140** A1133
27. Payne M C, Teter M P, Allan D C, Arias T A and Joannopoulos J D 1992 *Rev. Mod. Phys.* **64** 1045
28. Gonze X 1996 *Phys. Rev. B* **54** 4383
29. Rappe A M, Rabe K M, Kaxiras E and Joannopoulos J D 1990 *Phys. Rev. B* **41** 1227
30. Monkhorst H J and Pack J D 1976 *Phys. Rev. B* **13** 5188
31. Goedecker S, Teter M and Hutter J 1996 *Phys. Rev. B* **54** 1703
32. http://www.library.cornell.edu/nr/bookcpdf/c10-7.pdf
33. Hirshfeld F L 1977 *Theoret. Chim. Acta (Berl.)* **44** 129
34. Skorodumova N V, Baudin M and Hermansson K 2004 *Phys. Rev. B* **69** 075401
35. Dulaurent O, Courtois X, Perrichon V and Bianchi D 2000 *J. Phys. Chem. B* **104** 6001
36. Nishiyama H and Inoue Y 2005 *Surf. Sci.* **594** 156
37. Carlsson P -A, Österlund L, Thormählen P, Palmqvist A, Fridell E, Jansson J and Skoglundh M 2004 *J. Catal.* **226** 422
38. Hammer B, Morikawa Y and Nørskov J K 1996 *Phys. Rev. Lett.* **76** 2141
39. Bera P and Hegde M S 2010 *J. IISc.* **90:2** 299